
PERGAMON

Journal of Quantitative Spectroscopy & Radiative Transfer 82 (2003) 279–292

Journal of Quantitative Spectroscopy & Radiative Transfer

www.elsevier.com/locate/jqsrt

Hot methane spectra for astrophysical applications

Ray Nassar, Peter Bernath*

Department of Chemistry, University of Waterloo, 200 University Avenue West, Waterloo, Ont., Canada N2L 3G1

Received 14 September 2002; received in revised form 11 February 2003; accepted 11 February 2003

Abstract

We have recorded laboratory high resolution Fourier transform spectra of methane (CH_4) emission at 800, 1000 and 1273 K with an effective hot path length of 51 cm. The spectra span 2000–5000 cm^{-1} (resolution 0.020 cm^{-1}, nominal pressure 16.3 Torr) and 5000–6400 cm^{-1} (resolution 0.040 cm^{-1}, nominal pressure 79 Torr) for each temperature. We have determined line positions and intensities for 15 434, 22 163 and 25 727 emission lines in the 800, 1000 and 1273 K spectra, respectively. Positions have been calibrated to a 1σ accuracy of better than 0.001 cm^{-1} in the 2000–5000 cm^{-1} spectra and 0.003 cm^{-1} in the 5000–6400 cm^{-1} spectra based on the 2001 methane line list update in the HITRAN database. We have calculated absolute line intensity calibration factors for these lines based on HITRAN intensities scaled to the appropriate temperature. In addition, since some methane lines in our spectra appeared in absorption, we have directly used intensities calculated from HITRAN for 757, 839 and 1094 additional lines in the 800, 1000 and 1273 K spectra, respectively. We expect our new hot methane line lists to be useful for direct comparison and simulation of the spectral energy distribution from brown dwarfs and hot extrasolar giant planets, and may also be used for comparison with line lists generated by both ab initio quantum chemists and more traditional theoretical spectroscopists. Furthermore, the method we have developed for obtaining high temperature line lists can be applied to other molecules in the HITRAN database.

Keywords: Infrared; Emission spectra; High temperature; Atmosphere; Brown dwarfs; Extrasolar planets

1. Introduction

In this work, we present new high resolution spectroscopic line lists based on the infrared emission of methane (CH_4) at 800, 1000 and 1273 K. Currently, one of the best existing line lists for methane appears as the 2001 update to HITRAN [1–3] generated for low temperature applications such as

* Corresponding author. Tel.: +1-519-888-4814; fax: +1-519-746-0435.
E-mail address: bernath@uwaterloo.ca (P. Bernath).

0022-4073/03/$ - see front matter
doi:10.1016/S0022-4073(03)00158-4

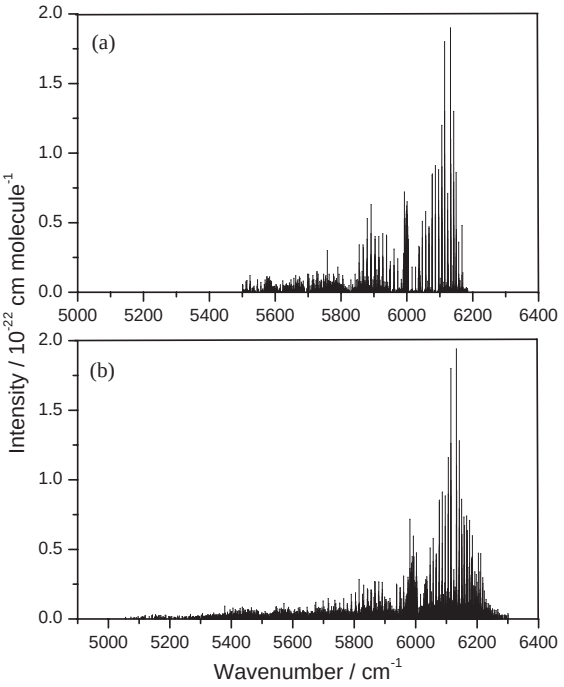

Fig. 1. Synthetic line spectra in the 5000–6400cm^{-1} region based on: (a) the HITRAN line list with intensities scaled to 1273 K, and (b) our line list which includes selected HITRAN lines. An explanation of how these spectra were obtained is given later, however, it is evident that simple extrapolation of room temperature HITRAN line lists will not adequately represent the hot methane spectra.

modeling transmission through Earth's atmosphere. Utilizing low temperature line lists for high temperature applications requires extrapolation of line intensities to the desired temperature, but a simple extrapolation does not account for missing transitions between highly excited levels. In particular, it leads to the omission of hot bands and often results in the incorrect simulation of the overall appearance of spectra, as illustrated in Fig. 1. Until this work, accurate high temperature methane line lists have not been readily available, yet are highly desirable for use by ab initio quantum chemists, more traditional theoretical spectroscopists and for a number of novel applications in astrophysics, such as the study of brown dwarfs and hot extrasolar planets.

Brown dwarfs are objects intermediate in mass between low-mass stars and giant planets. They are categorized into two classes, L and T [4,5], each with 10 subclasses as in the standard OBAFGKM stellar classification system. Near infrared spectra of T dwarfs are dominated by numerous methane and water bands [6]. L dwarf spectra are dominated by metal hydrides and CO, but the 3.3 μm methane ν_3 fundamental band begins to appear weakly at about $L5$ [7]. These methane bands have been identified by comparison with the spectra of Jupiter or with simulated spectra based on room temperature databases such as HITRAN [8] or GEISA [9]. The approximate temperature range for T dwarfs is 750 K $\leqslant T_{\mathrm{eff}} \leqslant$ 1300 K [5,10] and for L dwarfs, 1300 K $\leqslant T_{\mathrm{eff}} \leqslant$ 2200 K [4,11], but uncertainties remain as high as ±100 K for a particular dwarf and even higher for the boundaries of a class. It is well known that the equilibrium reaction $CO + 3H_2 \leftrightharpoons CH_4 + H_2O$ is temperature

dependent and because of methane's temperature sensitive chemistry, the ν_3 band may be an effective temperature indicator for late L dwarfs [12]. It has also been suggested that the abundance ratio between methane and CO at a given pressure, is a good indicator of the temperature of a brown dwarf [13]. The availability of laboratory hot methane spectra should prove to be useful for modeling brown dwarf atmospheres, and as the resolution of brown dwarf spectra improves, methane spectra may help determine better values for properties such as temperature, surface gravity and metallicity [14].

Until quite recently, the concept of planets orbiting other stars had been only theoretical, but over 100 extrasolar planets have been discovered within the past few years. Differences in size and proximity to their parent stars result in a wide range of surface temperatures, spanning about 150–1600 K [15]. Many of the extrasolar planets discovered so far are gas giants very close to their parent stars, such as HD 209 458b [16] and are believed to contain appreciable amounts of hot methane [16,17]. Although the atmosphere of HD 209 458b has been detected during transit, by the slight dimming of the sodium D line during photometric observation of the parent star [18], a spectrum of an extrasolar planet has not yet been recorded. Perhaps the importance of laboratory hot methane spectra may not be realized fully until the first spectra of extrasolar planets are directly recorded, which should be feasible in a few years.

2. Experimental work

To record laboratory spectra of methane at the temperatures desired, a portion of an alumina sample tube sealed with CaF_2 windows at each end, was heated in a high temperature tube furnace, as shown in Fig. 2. The temperature of the interior of the furnace was measured with a thermocouple and controlled to maintain a programmed temperature. One can assume that the portion of the tube within the furnace, and the interior of the furnace are at the same temperature. The ends of the tube were cooled to approximately room temperature with water-cooled copper coils to protect the rubber O-rings necessary to maintain vacuum. The flow of ultra-high purity methane through

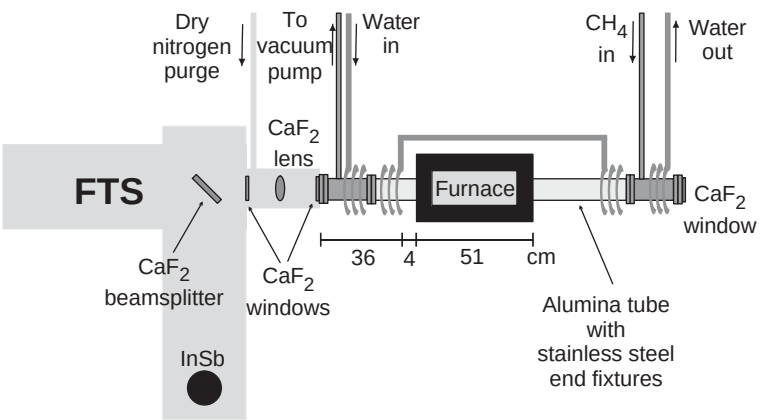

Fig. 2. Experimental setup.

Table 1
Some experimental conditions

Spectral range (cm^{-1})	Resolution (cm^{-1})	Temperature (K)	Pressure (Torr)	Flow rate (slpm[a])	Number of scans averaged
2000–5000	0.020	1273	16.3 ± 0.2	~ 1.5	100
2000–5000	0.020	1000	16.3 ± 0.2	~ 1.5	100
2000–5000	0.020	800	16.4 ± 0.2	~ 1.5	200
5000–6400	0.040	1273	79.2 ± 0.5	~ 0.4	380
5000–6400	0.040	1000	78.6 ± 0.5	~ 0.4	380
5000–6400	0.040	800	78.8 ± 1.0	~ 0.4	508

[a]slpm = standard litres per minute.

the tube (without a broadener or buffer gas) was controlled with a needle valve and monitored using a simple flowmeter. A flow system was used in order to prevent the build-up of impurities and loss of sample that usually occurs when scanning for long periods of time with a sealed heated system. Emission from the hot methane was focused using a CaF_2 lens and directed toward a Bruker® IFS 120 HR spectrometer equipped with a CaF_2 beamsplitter and a liquid nitrogen-cooled InSb detector. The chamber between the spectrometer and the CaF_2 lens was continuously purged with dry nitrogen gas to decrease absorption from atmospheric H_2O and CO_2. The spectra obtained consist mainly of emission lines, but for some spectra, a few absorption lines due to room temperature methane in the end of the tube are also present. In the spectra presented here, absorption was decreased compared to our earlier attempts by positioning the furnace so as to minimize the cold path length, and directing the methane flow toward the spectrometer allowing hot methane to flow into the cooled portion of the tube directly in front of the spectrometer.

At all three temperatures a strong signal was easily obtained for the bands in the 2000–5000 cm^{-1} region at a resolution of 0.020 cm^{-1}. In the 5000–6400 cm^{-1} region with a resolution of 0.040 cm^{-1}, the signal was relatively weak, resulting in satisfactory spectra at 1273 and 1000 K, but a very low signal-to-noise ratio at 800 K. Table 1 lists the number of scans, methane pressure and approximate flow rate for each spectral region.

3. Results and calculations

The laboratory spectra are shown in Fig. 3, for illustrative purposes only, since each panel is plotted on a different intensity scale. The general appearance of the spectra are similar for the corresponding regions but some qualitative differences in the intensity distribution can be seen. The upward peaks are due to hot methane emission and the downward peaks are due to absorption by room temperature methane in the cool end of the sample tube closest to the spectrometer. Bands are observed in the region of the prominent v_3 fundamental, the $2v_3$ and $2v_4$ overtones, and numerous combination bands. The spectra contain many hot bands that may not have been identified yet, but a detailed discussion of vibrational bands is not the subject of this paper and assigning these bands and lines will be left as a future pursuit.

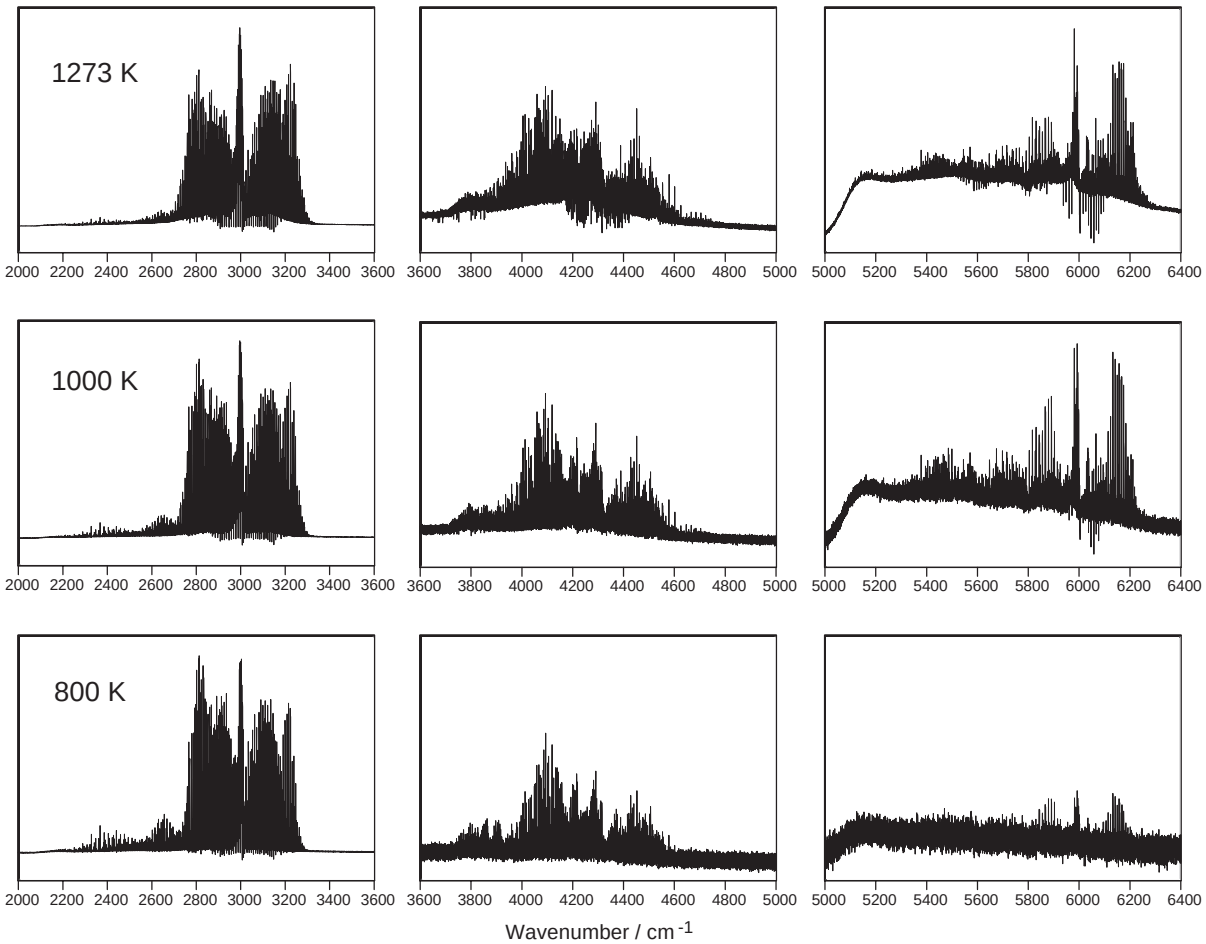

Fig. 3. Laboratory high resolution hot methane spectra. 1273 K spectra (top row), 1000 K (middle row) and 800 K (bottom row). Each panel is plotted with a different intensity scale, but qualitative differences are evident.

Raw spectra were apodized using a *Norton-Beer Weak* function [19,20], and post-zero-filled by a factor of 8. Line parameters were determined using a program called *WSpectra* [21]. Emission lines in the two spectra were fitted by non-linear least squares using Voigt lineshape functions, in three separate regions: 2000–3600, 3600–5000, and 5000–6400 cm^{-1} for each temperature. This resulted in nine line lists of emission lines with parameters including: line position, amplitude, full-width-at-half-maximum and area. The number of lines for each temperature and region can be seen in Table 2.

Absorption peaks were also fitted separately from emission, in six of the nine spectral regions. These cool lines were useful for calibrating the wave number scale with respect to the methane line lists found in the 2001 update to HITRAN [3,8]. Only strong, symmetric absorption lines were chosen for calibration, as these were assumed to be isolated, unblended lines with the most accurately determined line positions. For the 2000–5000 cm^{-1} region at 1273 K, 20 lines were

Table 2
Number of lines tabulated for each spectral region in the final line lists

Spectral region (cm^{-1})	Temperature (K)	Number of emission lines	Number of absorption lines	Combined number of lines
2000–3600	1273	15 731	709	16 440
3600–5000	1273	5919	218	6137
5000–6400	1273	4077	167	4244
Total	1273	25 727	1094	26 821
2000–3600	1000	15 566	751	16 317
3600–5000	1000	4915	25	4940
5000–6400	1000	1682	63	1745
Total	1000	22 163	839	23 002
2000–3600	800	12 348	673	13 021
3600–5000	800	2726	44	2770
5000–6400	800	360	43	400
Total	800	15 434	757	16 191

selected and compared to HITRAN resulting in a calibration factor of 0.99999832(19) or a shift of $-0.00588\ cm^{-1}$ at $3500\ cm^{-1}$. Similarly, for the 5000–6400 cm^{-1} region at 1273 K, 28 lines were used to determine a factor of 0.99999749(53) or a shift of $-0.014307\ cm^{-1}$ at $5600\ cm^{-1}$. (The numbers in parentheses, are one standard deviation on the last digits.) A significant number of lines from the 1000 and 800 K spectra indicated that their calibration factors should be the same as those for the corresponding 1273 K region as expected, since only the furnace temperature changed, with no changes to any relevant instrument settings.

In order to calibrate the intensity scale, first we converted laboratory emission intensities (in arbitrary units) to absorption using equation [22]:

$$S_{\text{absorption}} = \frac{S_{\text{emission}}}{v^3 \exp(-hv/kT)} \tag{1}$$

in which S is the intensity of a line and v is the frequency of the transition.

Goldman et al. [23] describe in detail, a number of factors that contribute to the intensity of a spectral line. However, to predict the intensity of a line at a different temperature, only the ratio of the line intensity expression at the desired temperature and the reference temperature are required (allowing many constants to cancel). Therefore, the intensity of a line at a new temperature may be predicted based on the HITRAN intensity in units of $cm^{-1}/(\text{molecule cm}^{-2})$ or cm molecule^{-1} using the following [23]:

$$S = S_0 \frac{Q_R(T_0)}{Q_R(T)} \frac{Q_V(T_0)}{Q_V(T)} \exp\left(\frac{E_{\text{low}}}{kT_0} - \frac{E_{\text{low}}}{kT}\right) \left[\frac{1 - \exp(-hv/kT)}{1 - \exp(-hv/kT_0)}\right] \tag{2}$$

in which S_0 is the intensity of a line at the reference temperature $T_0 = 296$ K, S the intensity of a line scaled to temperature T, Q_R the rotational partition function, Q_V the vibrational partition function and E_{low} the lower state energy.

Table 3
Intensity calibration factors

Spectral region (cm^{-1})	Temperature (K)	Intensity Calibration Factor (cm $molecule^{-1}$)	Relative Standard Deviation	Number of lines used
2000–3600	1273	4.29×10^{-12}	0.277	139
2000–3600	1000	3.95×10^{-12}	0.236	234
2000–3600	800	4.05×10^{-12}	0.301	257
3600–5000	1273	1.29×10^{-11}	0.364	86
3600–5000	1000	1.26×10^{-11}	0.394	180
3600–5000	800	1.26×10^{-11}	0.429	270
5000–6400	1273	3.36×10^{-12}	0.488	72
5000–6400	1000	3.09×10^{-12}	0.507	123
5000–6400	800	3.01×10^{-12}	0.449	62

Using the rigid rotor, harmonic oscillator approximation, the rotational partition function was scaled using the ratio [24]:

$$\frac{Q_R(T_0)}{Q_R(T)} = \frac{\sqrt{(\pi/ABC)(kT_0/hc)^3}}{\sqrt{(\pi/ABC)(kT/hc)^3}} = \left(\frac{T_0}{T}\right)^{3/2}, \tag{3}$$

where the three rotational constants A, B, and C are equal for a spherical top such as CH_4.

The vibrational partition function at each temperature was found using [24]

$$Q_V(T) = \prod_{i=1}^{N} \frac{1}{[1 - \exp(-E_i/kT)]^{d_i}} \tag{4}$$

in which d_i and E_i are the degeneracy and energy of the vibrational mode i, with the product taken for the four fundamental vibrational frequencies of the methane molecule: 2916.5, 1533.3, 3019.49, 1306.2 cm^{-1} [25]. The method of calculating the total partition function ratio $Q(T_0)/Q(T)$ described above agrees with empirical relationships for methane in Refs. [26,27] within 0.8% for a test temperature of 400 K, but these relationships cannot be used to directly verify our calculations up to 1273 K. Our values for the ratio are 0.14436, 0.073941, and 0.030586 at 800, 1000 and 1273 K, respectively. An alternate approach utilizing tabulated free energy functions [28,29] yields 0.14241, 0.072176, and 0.029286 for the same temperatures resulting in a maximum difference of 4.3% at 1273 K, confirming that our calculation is within a reasonable level of accuracy.

To determine absolute intensities for the laboratory spectra, individual laboratory lines were matched to HITRAN lines, and in some cases two or more very closely spaced lines from HITRAN were assumed to be unresolved, appearing as a single line in the high resolution laboratory spectrum. Strong, symmetrical laboratory lines were selected if possible but some weak or blended lines have also been included. The intensity calibration factors, number of lines used to obtain each factor and the relative standard deviations can be seen in Table 3. The factor quoted here is a multiplicative factor used to obtain an absolute intensity. It is applied after the conversion to absorbtion intensity has been carried out. Although peak area was available from our line-fitting program, we found that in practice peak height yielded a more reliable and consistent line intensity.

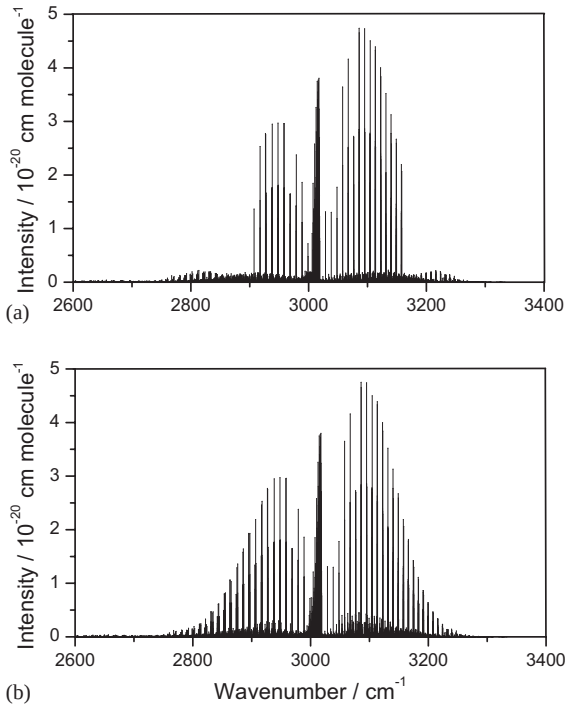

Fig. 4. Synthetic line spectra at 800 K based on: (a) laboratory emission lines converted to absorption and supplemented with HITRAN lines to account for observed strong absorption lines, and (b) laboratory emission lines converted to absorption and supplemented with HITRAN lines to account for observed strong absorption lines and any other calculated lines with intensities greater than the strongest experimental line. (Note the abrupt shape in the upper intensity distribution, uncharacteristic of real spectra.)

This likely occurred because area is much more sensitive than amplitude to errors in the position of the baseline, since the base of the peak makes such a large contribution to the total area. The accuracy of our absolute intensities is considered in the discussion below.

In order to produce a more complete line list, missing emission lines corresponding to the observed absorption lines had to be included, so we matched individual absorption lines from the laboratory spectra to individual HITRAN lines that had their intensities scaled to the appropriate temperature. For the 1201 absorption lines observed in our spectra, a few had no match in the HITRAN line list and thus were discarded. More frequently, absorption lines were matched to multiple unresolved HITRAN lines, resulting a total of 1260 temperature-scaled HITRAN lines added to our lists in this way. The HITRAN line lists occasionally have multiple lines at exactly the same line position (and sometimes even the same intensity) corresponding to multiple transitions. Although we do not list assignments for our lines, any absorption lines at the same wave number but corresponding to different transitions have been left separate in our lists and appear as repeated entries.

When synthetic line spectra are created from the laboratory emission line lists supplemented with absorption lines as described above, the strong lines greatly affect the overall shape of the spectral distributions. Although the added lines appear with the positions and intensity distribution characteristic of real spectra, it is obvious that they end far too abruptly in the 2000–3600 cm^{-1}

region (see Fig. 4). Evidently the lines that we observe are the superposition of hot emission lines and cool absorption lines. For those branches that connect to the ground vibrational levels the low-J lines appear in absorption and the high-J lines in emission and at some J value the emission and absorption will approximately cancel. The lines that we have added correct only for these low-J lines. To correct for the abrupt ending of branches that is uncharacteristic of real spectra, and to account for some of the lines that have diminished or even zero intensity, we have also added all lines in each region that should theoretically occur at intensities greater than the strongest observed line in that region, since these have the largest impact on the overall shape of the spectral distribution. This amounted to the addition of 1430 more lines, making a total of 2690 added HITRAN lines, which can be easily distinguished because they appear in our line lists without an amplitude, line width or area. By including the HITRAN lines in our line lists with slightly different fields, a user can easily sort the lines and remove the HITRAN lines if desired. An example of the HITRAN methane line list is given in Fig. 5 and an example of our line lists for the same region can be seen in Table 4. The exact number of lines added directly from HITRAN for each region is listed in Table 2. In total, our line lists contain nearly 66 000 lines, however, since most lines are observed at more than one temperature (Table 4) we estimate the number of unique lines at about 40 000, somewhat greater than the total number of lines at 1273 K (Table 2).

4. Discussion

Based on our calibration using HITRAN, we claim a 1σ absolute accuracy of better than 0.001 cm^{-1} for line positions in the 2000–5000 cm^{-1} spectra and 0.003 cm^{-1} for the 5000–6400 cm^{-1} spectra. We suggest an accuracy of a factor of two or better for our intensities. A higher level of accuracy for intensities would be desirable, but with absolute intensities spanning over four orders of magnitude, this is a reasonable result. Emission intensities are generally quite difficult to calibrate, with the limits on accuracy in our case arising from various sources. Firstly, no attempt was made to correct our experimental intensities for the variation in sensitivity that occurs over a given wave number range for an InSb detector. Secondly, for a hot polyatomic molecule such as methane, most spectral lines overlap, and fitting overlapping lines in a program such as *WSpectra* can produce some inaccurate intensities. Furthermore, although we estimate the accuracy of our measured temperature to be better than ± 10 K, we cannot ignore the fact that with our experimental setup, during a single scan we are not recording a spectrum of methane at a single temperature, but at some distribution of temperatures. The absorption lines due to cool methane make this point obvious, yet these are perhaps less problematic since they can be distinguished. Of the entire length of tube and fittings, the 51 cm fully contained in the furnace should be at the desired temperature. At the end of the tube between the furnace and the spectrometer, 36 cm of tube are at approximately room temperature, leaving about 4 cm between the furnace and spectrometer at intermediate temperatures (see Fig. 2). In the intermediate temperature portion, hot methane emission still occurs, contributing spectra with a slightly different intensity distribution but identical line positions. This results in some inaccuracy in line intensities for the final spectrum, but it should not be severe due to the very small path length and the lower total photon flux that occurs at lower temperatures. High temperature absorption measurements at a defined temperature would be superior to emission, but are technically more challenging to obtain.

```
  63 3038.034162 1.367E-27 0.000E+00.0342.0499 1500.10660.75-.005842 17 1419 7  E  19 5  E  332372521
  62 3038.044512 3.474E-27 4.516E-06.0390.0820 1779.68200.63-.006076  6  119A2 16  18A1  1  454352129
  63 3038.053223 1.681E-26 0.000E+00.0342.0499  861.03900.75-.005842 20 1415 1  A1 14 6  A2 332372521
  63 3038.058043 5.677E-28 0.000E+00.0342.0499 1982.87480.75-.005842 17 1422 7  E  22 5  E  332372521
  63 3038.079147 5.726E-28 0.000E+00.0342.0499 2127.37280.75-.005842 20 1423 1  E  23 1  E  332372521
* 61 3038.122600 1.670E-22 3.319E-05.0501.0810  815.14380.65-.003880  6  113A2 13  12A1  2  366312123
  61 3038.141508 8.351E-26 4.940E-08.0470.0684  950.30500.65-.006076  6  114F2 38  13F1  3  222312129
  63 3038.190209 1.102E-28 0.000E+00.0342.0499  791.05140.75-.005842 36 141414  E  13 8  E  332372521
  62 3038.232384 4.953E-27 2.652E-05.0550.0871 1976.74480.63-.006076  6  120F1 45  19F2  4  454352129
  63 3038.242445 1.201E-27 0.000E+00.0342.0499  705.80850.75-.005842 20 1414 2  E  13 1  E  332372521
  63 3038.278847 6.219E-29 0.000E+00.0342.0499  150.57880.75-.005842 17 14 6 3  E   5 5  E  332372521
  61 3038.306889 1.114E-25 9.968E-06.0550.0956 1975.01500.63-.006077  6  120E  30  19E   1  222312129
  61 3038.309931 6.714E-26 3.968E-08.0470.0684  950.13660.65-.006077  6  114F2 38  13F1  2  222312129
  61 3038.311750 1.668E-25 9.945E-06.0550.0871 1975.01270.63-.006077  6  120F1 44  19F2  2  222312129
  63 3038.313455 3.688E-26 0.000E+00.0342.0499 1316.57580.75-.005842 17 141615  E  1614  E  332372521
* 61 3038.320955 2.768E-25 9.904E-06.0550.1224 1975.00820.63-.006077  6  120A1 16  19A2  1  222312129
  63 3038.348938 6.151E-28 0.000E+00.0342.0499 2126.06860.75-.005842 20 1423 2  A1 23 0  A2 332372521
  63 3038.356110 6.896E-29 0.000E+00.0342.0499 1386.22090.75-.005842 37 141911  E  18 7  E  332372521
  63 3038.388262 9.113E-29 0.000E+00.0342.0499 1845.68320.75-.005842 20 142016  E  2013  E  332372521
  61 3038.390021 6.776E-25 0.000E+00.0320.0538 1491.50290.75-.006077 11  2 6E  31   5E   3  332332329
  63 3038.424737 3.867E-26 0.000E+00.0342.0499  284.54920.75-.005842 15 14 9 1  E   8 2  E  332372521
  63 3038.426561 7.081E-29 0.000E+00.0342.0499 1468.27600.75-.005842 17 1419 5  E  19 1  E  332372521
  63 3038.433921 4.501E-24 0.000E+00.0342.0499   24.64920.75-.005842 17 14 3 0  E   2 1  E  532372521
* 61 3038.448325 1.487E-24 0.000E+00.0450.1001 1729.88950.75-.006077 11  2 9A1 22   9A2  1  332332329
  63 3038.458605 9.052E-29 0.000E+00.0342.0499  532.95810.75-.005842 20 1412 5  E  11 4  E  332372521
  63 3038.465555 3.935E-28 0.000E+00.0342.0499 1729.43750.75-.005842 20 141917  E  1914  E  332372521
* 61 3038.498429 8.788E-20 4.854E-03.0635.0770   10.48160.65-.004500  8  1 2F2 10   1F1  1  566312123
  61 3038.505733 3.763E-25 0.000E+00.0440.0678 1488.91310.75-.006077 11  2 6F2 46   5F1  3  332332329
  63 3038.521811 7.820E-29 0.000E+00.0342.0499 1621.82210.75-.005842 17 1420 5  E  20 1  E  332372521
  63 3038.526892 1.804E-28 0.000E+00.0342.0499 2034.21260.75-.005842 20 1422 7  E  22 8  E  332372521
  63 3038.573832 6.342E-28 0.000E+00.0342.0499 2334.85620.75-.005842 17 142218  E  2217  E  332372521
  63 3038.574870 1.490E-26 0.000E+00.0342.0499  532.95810.75-.005842 20 1412 1  E  11 4  E  332372521
  63 3038.580788 2.463E-26 0.000E+00.0342.0499 1623.76750.75-.005842 17 141816  A1 1815  A2 332372221
  63 3038.593588 1.416E-26 0.000E+00.0633.0820  218.48970.75-.005843 15 14 8 2  E   7 1  E  334372521
  63 3038.595285 5.899E-25 0.000E+00.0633.0820  346.00760.75-.005843 15 14 9 7  E   8 7  E  532372521
  63 3038.598836 4.390E-27 0.000E+00.0633.0820 1056.89710.75-.005843 17 1416 4  E  16 2  E  332372521
  63 3038.601577 1.884E-25 0.000E+00.0633.0820  415.58810.75-.005843 20 1410 6  E   9 7  E  332372521
  61 3038.604839 1.873E-27 1.105E-09.0470.0684  949.84160.65-.006077  6  114F2 38  13F1  1  222312129
* 61 3038.605150 8.888E-25 0.000E+00.0390.0626 1879.88930.75-.006077 11  210F1 89  10F2  5  332332329
  62 3038.614490 1.247E-21 4.073E-03.0660.0803   31.44380.80-.006077  8  1 3F1 13   2F2  1   84352123
  61 3038.621657 1.658E-24 3.286E-07.0520.0814  814.64620.65-.006077  6  113A2 13  12A1  1  332312129
  63 3038.626310 3.153E-27 0.000E+00.0633.0820 1963.28970.75-.005843 17 142017  E  2016  E  332372521
  62 3038.628530 8.311E-22 4.073E-03.0624.0766   31.44360.80-.005560  8  1 3E   8   2E   1  566352123
* 61 3038.639720 2.256E-24 0.000E+00.0320.0538 1432.52400.75-.006077 11  2 5E  27   4E   2  332332329
  61 3038.642556 2.665E-27 2.409E-07.0550.0956 1977.19780.63-.006077  6  120E  31  19E   3  222312129
  61 3038.678000 8.689E-25 0.000E+00.0390.0618 1729.80860.75-.006077 11  2 9F1 68   9F2  2  332332329
  61 3038.690845 2.340E-24 0.000E+00.0440.0688 1680.75980.75-.006077 11  2 8F1 71   8F2  4  332332329
* 61 3038.726309 5.301E-25 0.000E+00.0390.0626 1994.36120.75-.006077 11  211F2 97  11F1  6  332332329
* 61 3038.762539 3.296E-24 0.000E+00.0470.0989 1596.72600.75-.006078 11  2 7A2 23   7A1  2  332332329
  63 3038.762803 1.502E-28 0.000E+00.0633.0820 1230.54130.75-.005843 15 1417 9  A1 17 6  A2 332372221
  61 3038.784400 1.937E-24 0.000E+00.0440.0678 1459.91190.75-.006078 11  2 5F1 49   5F2  2  332332329
* 61 3038.808540 5.700E-25 0.000E+00.0290.0504 1729.76150.75-.006078 11  2 9E  44   9E   2  332332329
  63 3038.829798 1.601E-28 0.000E+00.0462.0641 1117.25130.75-.005844 20 1417 0  E  16 7  E  334372521
  63 3038.841611 1.496E-27 0.000E+00.0462.0641  431.61510.75-.005844 20 1411 2  E  10 2  E  332372521
  61 3038.844621 5.221E-25 0.000E+00.0320.0538 1491.50290.75-.006078 11  2 6E  32   5E   3  332332329
  61 3038.860419 2.376E-27 1.432E-07.0550.0871 1977.21510.63-.006078  6  120F2 45  19F1  5  222312129
  63 3038.904373 3.910E-27 0.000E+00.0462.0641  994.12780.75-.005844 15 141510  E  15 7  E  332372521
  61 3038.906437 1.750E-24 0.000E+00.0440.0678 1491.32190.75-.006078 11  2 6F2 47   5F1  4  332332329
  63 3038.946227 6.053E-27 0.000E+00.0462.0641  921.95380.75-.005844 17 1415 4  A1 14 9  A2 332372521
  63 3038.947979 6.077E-27 0.000E+00.0462.0641  921.95380.75-.005844 17 1415 4  A2 14 9  A1 332372521
```

Fig. 5. A 1 cm^{-1} sample of the HITRAN methane line list. The first three columns are *Molecule/Isotopomer*, *Line position*, and *Intensity*, where $^{12}CH_4$ is molecule/isotopomer 61 in HITRAN. An explanation of all other columns is given earlier in this issue [8]. The asterisks (*) denote lines that were observed in our experimental spectra.

Calculating integrated intensities can be used as a rough validation of our intensity determination. The integrated intensities of room temperature methane bands have been determined by many groups in the past, as described in a review by Kim [30]. A recent determination for the 3–5 μm (2000–3333 cm^{-1}) region, of the $^{12}CH_4$ isotopomer arrived at a value of 1.122×10^{-17} cm $molecule^{-1}$ at

Table 4
A 1 cm^{-1} sample of our line lists at each temperature for the same region as the HITRAN list shown in Fig. 5

	Wavenumber (cm^{-1})	Intensity (cm $molecule^{-1}$)	Amplitude (a.u.)	Full width (cm^{-1})	Eq. width (a.u.)
800 K	3038.028622	3.72×10^{-23}	0.00109	0.016452	0.019
	3038.054737	5.73×10^{-23}	0.00168	0.006485	0.012
	3038.089680	4.57×10^{-23}	0.00134	0.011260	0.016
	3038.121776	2.80×10^{-22}	0.00822	0.020758	0.182
	3038.170229	4.26×10^{-23}	0.00125	0.028796	0.050
	3038.286596	5.80×10^{-23}	0.00170	0.040725	0.074
	3038.448756	6.38×10^{-23}	0.00187	0.035696	0.071
	3038.498429	1.30×10^{-20}			
	3038.538967	1.00×10^{-22}	0.00294	0.022130	0.069
	3038.603785	7.40×10^{-23}	0.00217	0.045890	0.106
	3038.639924	5.87×10^{-23}	0.00172	0.019724	0.036
	3038.685432	1.64×10^{-22}	0.00481	0.024227	0.129
	3038.723566	6.51×10^{-23}	0.00191	0.005832	0.012
	3038.760128	8.08×10^{-23}	0.00237	0.046797	0.174
	3038.803031	2.66×10^{-23}	0.00078	0.024079	0.024
	3038.896893	2.65×10^{-22}	0.00778	0.033793	0.280
	3038.973315	1.51×10^{-22}	0.00444	0.027050	0.128
1000 K	3038.120023	1.64×10^{-22}	0.01475	0.024944	0.521
	3038.169770	4.79×10^{-23}	0.00430	0.021084	0.097
	3038.203046	1.63×10^{-23}	0.00146	0.023254	0.036
	3038.286758	6.69×10^{-23}	0.00600	0.037464	0.239
	3038.498429	6.65×10^{-21}			
	3038.540320	9.32×10^{-23}	0.00836	0.019267	0.171
	3038.596851	6.70×10^{-23}	0.00601	0.027457	0.188
	3038.642035	4.67×10^{-23}	0.00419	0.017683	0.099
	3038.684932	1.96×10^{-22}	0.01755	0.025238	0.567
	3038.723274	5.71×10^{-23}	0.00512	0.006477	0.049
	3038.753539	8.83×10^{-23}	0.00792	0.030800	0.346
	3038.796438	5.98×10^{-23}	0.00536	0.049406	0.416
	3038.896236	3.20×10^{-22}	0.02872	0.035887	1.118
	3038.973872	1.83×10^{-22}	0.01645	0.030413	0.532
1273 K	3038.113055	8.55×10^{-23}	0.01804	0.046161	1.299
	3038.169486	4.88×10^{-23}	0.01029	0.021677	0.237
	3038.204781	2.31×10^{-23}	0.00488	0.025423	0.132
	3038.284136	6.46×10^{-23}	0.01362	0.032546	0.472
	3038.318484	3.40×10^{-23}	0.00718	0.031351	0.239
	3038.498429	2.70×10^{-21}			
	3038.683734	1.48×10^{-22}	0.03128	0.023377	0.778
	3038.772848	4.68×10^{-23}	0.00986	0.091392	1.296
	3038.895711	2.83×10^{-22}	0.05958	0.035808	2.271

Note the easily distinguishable absorption line at 3038.498429 cm^{-1}.

Table 5
Intensity sums from our line lists and from temperature-scaled HITRAN line lists

Spectral region (cm^{-1})	Temperature (K)	Intensity sum (cm $molecule^{-1}$)	HITRAN intensity sum (cm $molecule^{-1}$)	Ratio to HITRAN
2000–3600	1273	4.89×10^{-18}	4.76×10^{-18}	1.03
3600–5000	1273	2.40×10^{-19}	2.07×10^{-19}	1.16
5000–6400	1273	2.59×10^{-20}	1.48×10^{-20}	1.75
2000–3600	1000	7.66×10^{-18}	7.51×10^{-18}	1.02
3600–5000	1000	3.80×10^{-19}	3.79×10^{-19}	1.00
5000–6400	1000	3.34×10^{-20}	3.09×10^{-20}	1.08
2000–3600	800	7.77×10^{-18}	9.53×10^{-18}	0.82
3600–5000	800	4.56×10^{-19}	5.57×10^{-19}	0.82
5000–6400	800	3.33×10^{-20}	5.11×10^{-20}	0.65

296 K [31]. Inclusion of the $^{13}CH_4$ and $^{12}CH_3D$ isotopomers at their natural abundances would increase the total intensity by less than 2%. A very good approximation to the integrated intensity can be found by taking the sum of HITRAN intensities at 296 K which yields 1.129×10^{-17} cm $molecule^{-1}$ for the main isotopomer over the 2000–3333 cm^{-1} range. Scaling the HITRAN intensities to 800, 1000 and 1273 K and summing each again, causes a decrease in the total intensity for any region as temperature increases, as seen in Table 5. A comparison of our intensity sums for both the emission and absorption lines to the temperature-scaled HITRAN intensity sums of the three regions at three temperatures, yields results from 65% to 175% of the scaled HITRAN sum. We attribute the values lower than 100% to missing weak lines due to the low signal-to-noise ratio obtained during measurement, most notably for the 800 K line list in the 5000–6400 cm^{-1} region, and to a lesser extent in other regions as well. Elsewhere, the intensity sums are greater than or equal to the value predicted by scaling HITRAN to the appropriate temperature. We acknowledge the fact that a small error in these intensity sums occurs because our method of adding absorption lines could occasionally include certain lines in both emission and absorption, however, we roughly estimate that this occurs for fewer than 300 lines out of over 66 000 lines in total (most being Q-branch lines around 3000 cm^{-1}) or an error of 3% in each of the 2000–3600 cm^{-1} regions and negligible for the others. Hence, we cite the greater than 100% intensity sum ratios and the general trend observed in Table 5 as evidence that simply scaling HITRAN to high temperatures gives an inadequate representation of hot spectra, likely attributable to the omission of hot bands. However, the combination of lines from laboratory spectra supplemented by properly selected HITRAN lines to correct for absorption, produces a much better result.

Other approaches to obtaining high temperature methane spectra include a fully ab initio approach to the prediction of high temperature methane spectra by Schwenke and Partridge [31] and simulations by the extrapolation of room temperature data using sophisticated Hamiltonians developed at the Université de Bourgogne [32]. Our experimental spectra are valuable for comparison with these predictions to test and validate the models and one of our earlier 1273 K spectra is being used for this purpose by the Université de Bourgogne group [33]. Very recently, a vibrational self-consistent field method was applied to methane in order to predict highly excited vibration-rotation energy levels [34,35].

An electronic version of our line lists for hot methane may be downloaded from *http://bernath.uwaterloo.ca/CH4*. A preliminary uncalibrated hot methane spectrum from our group has already been used to identify hot methane lines produced by the impact of comet Shoemaker–Levy 9 with Jupiter [36]. We believe that in the future, our line lists will be effective for direct comparison and simulation of the spectral energy distribution from brown dwarfs and hot extrasolar giant planets, as well as other high temperature applications. Furthermore, the method we have developed to create this line list can be utilized for other molecules in the HITRAN database that may be needed for the studies of high temperature phenomena.

Acknowledgements

Funding for this work was provided by the Natural Sciences and Engineering Research Council of Canada with partial support provided by the NASA Laboratory Astrophysics program. We would like to thank Tsuyoshi Hirao and Keith Tereszchuk for their help and we acknowledge the work of Frank Charron who recorded a preliminary hot methane spectrum.

References

[1] Féjard L, Champion JP, Jouvard JM, Brown LR, Pine AS. J Mol Spectrosc 2000;201:83.
[2] Hilico J-C, Robert O, Loëte M, Toumi S, Pine AS, Brown LR. J Mol Spectrosc 2001;208:1.
[3] Brown L, Benner DC, Champion JP, Devi VM, Fejard L, Gamache RR, Gabard T, Hilico JC, Lavorel B, Loëte M, Mellau GCh, Nikitin A, Pine AS, Predoi-Cross A, Rinsland CP, Robert O, Sams RL, Smith MAH, Tashkun SA, Tyuterer VlG. JQSRT, doi:10.1016/S0022-4073(03)00155-9.
[4] Kirkpatrick JD, Reid IN, Liebert J, Cutri RM, Nelson B, Beichman CA, Dahn CC, Monet DG, Gizis JE, Skrutskie MF. Astrophys J 1999;519:802.
[5] Burgasser AJ, Kirkpatrick JD, Brown ME, Reid IN, Burrows A, Liebert J, Matthews K, Gizis JE, Dahn CC, Monet DG, Cutri RM, Skrutskie MF. Astrophys J 2002;564:421.
[6] Strauss MA, Fan X, Gunn JE, Leggett SK, Geballe TR, Pier JR, Lupton RH, Knapp GR, Annis J, Brinkmann J, Crocker JH, Csabai I, Fukugita M, Golimowski DA, Harris FH, Hennessy GS, Hindsley RB, Ivezic Ž, Kent S, Lamb DQ, Munn JR, Newburg H, Rechenmacher R, Scheider DP, Smith JA, Stoughton C, Tucker DL, Waddell P, York DG. Astrophys J 1999;522:L61.
[7] Noll KS, Geballe TR, Leggett SK, Marley MS. Astrophys J 2000;541:L75.
[8] Rothman LS, Barbe A, Benner DC, Brown LR, Camy-Peyret C, Carleer MR, Chance K, Clerbaux C, Dana V, Devi VM, Fayt A, Flaud J-M, Gamache RR, Goldman A, Jacquemart D, Jucks KW, Lafferty WJ, Mandin J-Y, Massie ST, Nemtchinov V, Newrham DA, Perrin A, Rinsland CP, Schroeder J, Smith KM, Smith MAH, Tang K, Toth RA, Vander Auwera J, Varanasi P, Yoshino K. JQSRT, doi:10.1016/S0022-4073(03)00146-8.
[9] Jacquinet-Husson N, Arié E, Ballard J, Barbe A, Bjoraker G, Bonnet B, Brown LR, Camy-Peyret C, Champion JP, Chédin A, Chursin A, Clerbaux C, Duxbury G, Flaud J-M, Fourrié N, Fayt A, Graner G, Gamache R, Goldman A, Golovko Vl, Guelachvili G, Hartmann JM, Hilico JC, Hillman J, Lefèvre G, Lellouch E, Mikhaïlenko SN, Naumenko OV, Nemtchinov V, Newnham DA, Nikitin A, Orphal J, Perrin A, Reuter DC, Rinsland CP, Rosenmann L, Rothman LS, Scott NA, Selby J, Sinitsa LN, Sirota JM, Smith AM, Smith KM, Tyuterev VlG, Tipping RH, Urban S, Varanasi P, Weber M. JQSRT 1999;62:205.
[10] Burgasser AJ, Kirkpatrick JD, Cutri RM, McCallon H, Kopan G, Gizis JE, Liebert J, Reid IN, Brown ME, Monet DG, Dahn CC, Beichman CA, Skrutskie MF. Astrophys J 2000;531:L57.
[11] Geballe TR, Knapp GR, Leggett SK, Fan X, Golimowski DA, Anderson S, Brinkmann J, Csabai I, Gunn JE, Hawley SL, Hennessy G, Henry TJ, Hill GJ, Hindsley RB, Ivezic Ž, Lupton RH, McDaniel A, Munn JA, Narayanan VK, Peng E, Pier JR, Rockosi CM, Schneider DP, Smith JA, Strauss MA, Tsvetanov I, Uomoto A, York DG, Zheng W. Astrophys J 2002;564:461.

[12] Geballe TR, Noll KS, Leggett SK, Knapp GR, Fan X, Golimowski D. Infrared spectroscopy of brown dwarfs: the onset of CH_4 absorption in L dwarfs and the L/T transition. In: Jones HRA, Steele IA, editors. Ultracool dwarfs: new spectral types L and T. Berlin: Springer, 2001. p. 83–91.
[13] Lodders K, Fegley Jr B. Icarus 2002;155:393.
[14] Sengupta S, Krishan V. Astron Astrophys 2000;358:L33.
[15] Sudarsky D, Burrows A, Pinto P. Astrophys J 2000;538:885.
[16] Charbonneau D, Brown TM, Latham DW, Mayor M. Astrophys J 2000;529:L45.
[17] Weidemann G, Deming D, Bjoraker G. Astrophys J 2001;546:1068.
[18] Charbonneau D, Brown TM, Noyes RW, Gilliland RL. Astrophys J 2002;568:377.
[19] Norton HR, Beer R. J Opt Soc Am 1976;3:259–64.
[20] Norton HR, Beer R. Erratum. J Opt Soc Am 1977;3:419.
[21] Carleer MR. WSpectra: a Windows program to accurately measure the line intensities of high-resolution Fourier transform spectra. Remote Sensing of Clouds and the Atmosphere V, Proceedings of SPIE-International Society for Optical Engineering, 2001. vol. 4168, p. 337.
[22] Bernath PF. Spectra of atoms and molecules. New York: Oxford University Press, 1995.
[23] Goldman A, Dang-Nhu M, Bouanich JP. JQSRT 1989;41:17.
[24] Herzberg G. Molecular spectra and molecular structure II. Infrared and Raman spectra of polyatomic molecules. Malabar, FL: Kreiger Publishing, 1991.
[25] Herzberg G. Molecular spectra and molecular structure III. Electronic spectra and electronic structure of polyatomic Molecules. Malabar, FL: Kreiger Publishing, 1991.
[26] Fischer J, Gamache RR. JQSRT 2002;74:273.
[27] Gamache RR, Kennedy S, Hawkins R, Rothman LS. J Mol Struct 2000;517–8:407.
[28] Gurvich LV, Veyts IV, Alcock CB, editors. Thermodynamic properties of individual substances, vol. 1, part 1, 4th ed. New York: Hemisphere Publishing Corporation, 1989. p. 11–2.
[29] Gurvich LV, Veyts IV, Alcock CB, editors. Thermodynamic properties of individual substances, vol. 2, part 2, 4th ed. New York: Hemisphere Publishing Corporation, 1989. p. 36.
[30] Kim K. JQSRT 1987;37:107.
[31] Schwenke DW, Partridge H. Spectrochim Acta, Part A 2001;57:887.
[32] Wegner Ch, Champion J-P. JQSRT 1998;59:471.
[33] Borysov A, Champion J-P, Jørgensen UG, Wenger Ch. Mol Phys 2002;22:3585.
[34] Cassam-Chenaï P, Liévin J. J Quant Chem 2003;93:245.
[35] Cassam-Chenaï P, JQSRT 2003; doi:10.1016/S0022-4073(03)00157-2.
[36] Dinelli BM, Miller S, Achilleos N, Lam HA, Cahill M, Tennyson J, Jagod M-F, Oka T, Hilico J-C, Geballe TR. Icarus 1997;126:107.